ELSEVIER

Journal of Chromatography A, 806 (1998) 239–250

JOURNAL OF CHROMATOGRAPHY A

Hydrophobic interaction chromatography coupled with dynamic surface tension detection for the determination of surface active species in protein formulations

Nels A. Olson[a], Kristen J. Skogerboe[b], Robert E. Synovec[a,*]

[a]*Department of Chemistry, Box 351700, University of Washington, Seattle, WA 98195-1700, USA*
[b]*Department of Chemistry, Seattle University, Seattle, WA 98122, USA*

Received 19 September 1997; received in revised form 7 January 1998; accepted 7 January 1998

Abstract

The measurement and analysis of surface active species (surfactants) in protein formulations by hydrophobic interaction chromatography (HIC) coupled with gradient elution and dynamic surface tension detection (DSTD) is presented. The DSTD is based upon the measurement of the pressure inside a repeating drop formed when the eluate of a liquid chromatographic separation flows through the end of a pointed stainless steel capillary tube. The DSTD provides a measure of the dynamic surface tension at the air–liquid interface, and in some applications, information on adhesive interactions at the solid–liquid interface. A method for extraction of the desired surface tension signal from the raw pressure data is reported. High-salt gradient HIC separations are demonstrated and shown to be compatible with DSTD. With the gradient pumping system, optimum signal sensitivity and stability (low noise) were achieved when the pressure measurement is taken when the drop size is a minimum. Implementation of HIC–DSTD with salt gradient elution revealed that the noise of DSTD was slightly higher in the gradient mode, due to higher flow-rate imprecision with a dual pump system, as compared to employing isocratic elution. The combination of HIC with DSTD provides a selective methodology for the analysis of surface active species in commercially available protein formulations. Calibration of the HIC–DSTD instrument was achieved using surface active and/or surface tension lowering standards (2-propanol, 1-hexanesulfonic acid, and *N*-decyl-*N*,*N*-dimethyl-3-ammonio-1-propane-sulfonate), that were separated by gradient HIC with sequential ultraviolet (UV) absorbance detection (at 250 nm) and DSTD. The standards were detected only by DSTD. A commercial ribonuclease A formulation was analyzed. The data revealed one primary peak by UV absorbance detection, while two significant peaks with retention times earlier than the primary UV absorbance peak were observed with the DSTD. The identity of the primary UV absorbing peak was confirmed as ribonuclease A by enzyme assay. The first two surface active species observed with the DSTD show no enzyme activity. The utility of the DSTD coupled with HIC separations is demonstrated, opening several new avenues of investigation for the researcher interested in gaining a new perspective on the surface active species in complex biological samples.

Keywords: Hydrophobic interaction chromatography; Dynamic surface tension detection; Surface tension detection; Detection, LC; Surfactants; Ribonucleases; Proteins

1. Introduction

Surfactants play a key role in many chemical

*Corresponding author

0021-9673/98/$19.00
PII S0021-9673(98)00017-X

systems, so the analysis of surfactants is becoming increasingly important [1,2]. Surfactants are used in areas as diverse as food additives, paint spreaders, chromatographic mobile phase modifiers, cleaners and degreasers, pharmaceutical delivery systems and hydrocarbon remediation agents. Surfactant analyses are performed with high-performance liquid chromatography (HPLC) by reversed-phase, size-exclusion or ion-exchange separation mechanisms with a variety of detection schemes. For example, anionic surfactants such as alkyl sulfates or alkyl sulfonates are readily separated by reversed-phase HPLC [3]. Since many surfactants lack the chromophore necessary for direct absorbance detection, conductivity detection is often applied [3]. For aliphatic anionic surfactants (e.g., dodecyl sulfate) conductivity detection still suffers from relatively poor detectabilities, and has prompted the development of indirect absorbance and indirect conductivity detection methods for their analysis [4]. The chromatographic methods mentioned above are useful for the separation and detection of surfactants. Unfortunately, these methods do not directly probe the unique properties of the surfactants present in a separated sample. Thus, selective properties of surfactants, such as surface tension lowering ability and adhesion interactions, are not provided by these current HPLC analysis methods for surfactants.

Owing to the importance of surfactants in many chemical systems, there is considerable need to develop methods that measure the surfactant properties directly. An important goal of surfactant analysis is to couple selective detection with HPLC or related separation techniques. Work reported in this manuscript focuses on this goal. The most promising instruments for dynamically measuring surfactant properties are based upon measuring interfacial properties of drops or bubbles [5–14]. Although not applied to HPLC, a surface tension detection method based upon pressure measurements was reported in which a drop of a specific size was modulated by forward and reverse flow, while measuring the pressure of the drop with time [5]. This method provided kinetic data with regard to surfactant interactions at the air–liquid interface, yet required a relatively large sample volume and long equilibration time [6]. Others have related the technique of pressure-modulated air bubbles to the study of pulmonary surfactant [7], and other complex biomedical samples [8–10]. Work related to surface tension detection includes a multi-wavelength fiber-optic based drop analyzer [11], and a drop analyzer for interfacial liquid–liquid surface tension [12]. Recently, MacLeod and Radke reported that the pressure and size of continually expanding and detaching liquid drops at constant forward flow was related to the interfacial tension in both liquid–liquid and liquid–gas environments [13,14]. Their instrument was not designed for HPLC, but the concept was ideally suited for further development for HPLC detection (see below). These various methods have limitations for probing surfactant properties when one considers key requirements for HPLC detection, specifically a compatible detection volume, a suitable, steady forward flow-rate, a time constant that is suitable to the HPLC separation time-scale, and the general development of the instrument in the context of HPLC instrumentation and methodology.

We have been developing a dynamic surface tension detection (DSTD) system based upon the capillary-drop method [15–19] that is compatible with HPLC. Recently, we reported a multi-dimensional DSTD system that dynamically measures the pressure across the air–liquid interface of drops that repeatedly grow and detach from a pointed capillary tip [19]. Both liquid–air and liquid–solid (adhesional) interfacial tension contributions [13,14,20] to the multi-dimensional signal were observed and analyzed. Inherent challenges in designing the pressure-based DSTD system were the formation of a reproducible small drop volume, so as not to introduce additional chromatographic band broadening and the minimization or elimination of hysteresis or carryover at the capillary tip. Our instrument design has addressed these design issues, and shows promise as a sensitive and selective method of surface tension detection for flowing liquid samples such as with HPLC [19]. To that end, the first HPLC separations performed with DSTD where done using aqueous size-exclusion chromatography (SEC) [15,16,19]. Our ongoing goal is to expand the applicability of surfactant monitoring, in regard to both detector development and HPLC separation methods. This work describes the application and evaluation of DSTD with hydrophobic interaction chromatography (HIC), where gradient elution with

a high salt concentration mobile phase is required. The use of DSTD with gradient elution HIC is novel and broadens the scope of this detector, and the analytical capabilities of HIC.

We demonstrate HIC–DSTD in the analysis of biological materials, such as protein enzyme formulations. Due to the purification techniques used for many proteins the presence of surfactants in commercial formulations is ubiquitous. We selected 85% pure ribonuclease A as a model for studying the application of DSTD to protein formulations. While the purity of this ribonuclease A is suitable for many applications, the presence of contaminating surfactants could have a profound impact on the activity of the protein and its structural stability [21–23]. These concerns may necessitate the analysis of biomolecule preparations for surface active chemical species. In this study, HIC is coupled with UV absorbance detection in-series with DSTD for the analysis of surfactant standards and commercial protein preparations. The two detectors in series provide complimentary information. We have evaluated the DSTD performance with respect to a gradient pumping system, and have developed a data analysis technique that optimizes the performance of the instrument. In an effort to further characterize pressure-based DSTD, we have included microscopic observation of drop formation correlated to the measurement of the pressure within each liquid drop. Drops of different size and shape have different mechanical stability, that can be influenced by fluctuations in the flow-rate of the system. Consideration of drop shape and flow-rate precision shows that the drop maximum pressure signal has the optimum signal-to-noise ratio (S/N) for the gradient pumping system applied.

2. Theory of instrument design and operation

The DSTD system is based upon a pressure sensor whose signal is related to the surfactant properties of a given aqueous sample. The sensor is mounted in the side arm off the main flow capillary, as in Fig. 1. Note that the sensor is the same variety used in HPLC viscosity detector design, so the technology is well established. For the implementation of the detector to HPLC the mobile phase flows through a short capillary and forms drops at a specially machined tip (Fig. 1). The optimized design of the instrument covered in our previous publication [19] requires selecting the proper capillary composition, length, radius and volumetric flow-rate so the total signal is composed of the proper combination of surface tension and adhesion while minimizing the viscosity background providing a good S/N and chemical selectivity.

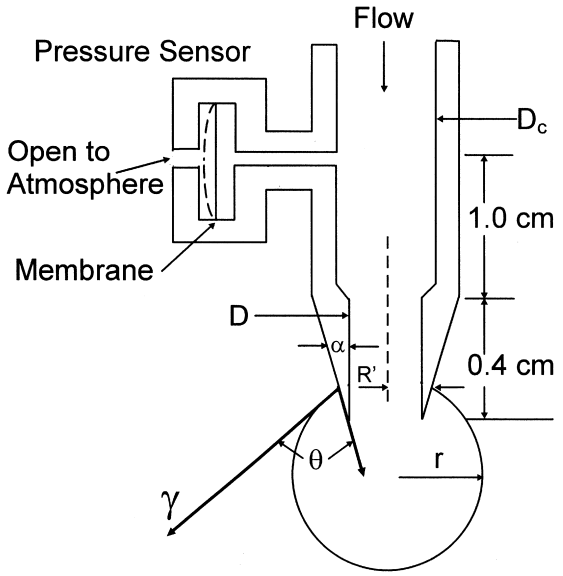

Fig. 1. Illustration of the pressure sensor, and a drop that forms at the pointed capillary tip with a tapered angle, α. Deformation of the sensor membrane (solid line to dashed line) is converted into an electrical signal. Diameters, $D=0.007$ and $D_c=0.020$ in., and radii, R' and drop radius r are described in the text. Analytes separated by the HIC column pass through the stainless steel capillary where a repeating drop is formed at the tip. A sensor measures the pressure as a function of time, $P(T)$. The liquid–air surface tension, γ, and mechanical equilibrium contact angle, θ, are defined for a drop early in its growth.

Drops forming at the capillary tip are approximately spherical for much of their growth. The liquid–air surface tension, γ, for a drop of radius r is related to the raw pressure signal $P(T)$, that is a pressure *difference* across the liquid–air interface of the drop relative to atmospheric pressure [13,19], with

$$P(T) = 2\gamma(T)/r(T) + C \quad (1)$$

where the P, γ and r are all a function of time, T, and

C accounts for viscous losses in the capillary tubing and the relative position of the sensor from the capillary tip [13]. Time T corresponds to the total chromatogram run time since injection. The raw pressure signal is composed of a large number of drops, and Eq. (1) can be decomposed into the individual drop profiles according to drop number n, and an individual time axis for each drop, t_d,

$$P(t_d,n) = 2\gamma(t_d,n)/r(t_d,n) + C \quad (2)$$

Eq. (2) indicates that the pressure sensor measurement has the potential to provide two-dimensional data, analogous to measuring the absorbance spectrum on-the-fly with HPLC. However, in this application we are interested in obtaining single-channel chromatographic data at optimum S/N, using a single measure of $\gamma(t_d,n)$ from each drop. Calibration of the chromatographic time axis requires consideration of the drop detachment process.

The condition for drop detachment is achieved when the forces due to the liquid clasping the tip of the capillary are overcome by the force of gravity on the mass of the drop. For a pointed capillary tip a reasonable model that describes the relationship between surface tension, adhesion and the force of gravity at the time of drop detachment is

$$t_{drop}(n) = 2\pi R'[\gamma(t_{drop}(n))][1 + \cos\theta(n)\cos\alpha]/[\rho(n)FG] \quad (3)$$

where $t_{drop}(n)$ is the maximum t_d for each drop n defined by each decomposed profile in Eq. (2), R' is the effective radius at which the liquid clasps the capillary tip, α is the angle of the tapered capillary tip, θ is the mechanical equilibrium contact angle of the eluate with the capillary surface, i.e., well prior to drop elongation (see Fig. 1), ρ is the density of the drop liquid, F is the volumetric flow-rate, and G is the gravitational force constant. Note that θ includes the adhesion effect, that for a flat capillary tip is not observed in most cases [13,19,20]. In work reported here, we do not make extensive use of the drop time for obtaining surface tension information, yet future investigations may find the adhesion information useful. Indeed, in previous work we demonstrated the ability to obtain two-dimensional chromatographic data from the decomposed drop profiles (Eq. (2)) by coupling DSTD to SEC [19]. For single-channel data the running time axis is obtained by the running total integration of Eq. (3),

$$t(n) = t = \sum_{i=1}^{n} t_{drop}(i) \quad (4)$$

where the time axis is simply denoted by t and it is understood that one pressure reading per drop is stored to obtain the single-channel data, in contrast to the raw data set (Eq. (1)) in which the entries along the time axis T are further dependent upon the data collection rate.

Eq. (2) provides the framework to obtain surface tension and adhesion information, coupled to their kinetic dependencies during drop formation and detachment. However, our current instrument design is optimized for high sensitivity by choosing a sensor membrane that exhibits a fairly long equilibration time between drop detachment and growth of the next drop. This design minimizes any kinetic effects, so a good approximation is that liquid–air surface tension γ measured at any point along an individual drop growth is essentially constant. In terms of Eqs. (2)–(4), for a given drop n,

$$\gamma(t_d,n) \sim \gamma(t_{drop}(n)) \sim \gamma(t) \quad (5)$$

Where $\gamma(t)$ is an average value for a given drop, but this average value can change from one drop to the next, as is the case with an eluting chromatographic peak. This approximation has been shown to be acceptable for many surfactants [19].

Maximum sensitivity for single-channel chromatographic data is obtained by considering Eqs. (1)–(5), and is obtained at the point of minimum drop radius, r_{min},

$$P(t)_{max} = 2\gamma(t)/r_{min} + C \quad (6)$$

where $P(t)_{max}$ is the maximum pressure signal for each drop. Note that the minimum radius is a constant and not dependent on time since it is defined by the capillary geometry, i.e., the inside radius of the capillary tip. The approximation in Eq. (5) is valid in Eq. (6) to the extent that the average $\gamma(t)$ is equal to, or slightly less than $\gamma(t_d,n)$ measured at $P(t)_{max}$. In HPLC, one is also interested in the analyte signal relative to the mobile phase (subscript mp),

$$\Delta P(t)_{max} = P(t)_{max} - P(t)_{max,mp} = 2\Delta\gamma(t)/r_{min} \quad (7)$$

that predicts a maximum drop pressure change $\Delta P(t)_{max}$ for a given change in eluate surface tension, $\Delta\gamma$, at the constant r_{min}. Conversely, just prior to the drop detaching due to the force of gravity, the radius has grown to a maximum value, and

$$P(t)_{min} = 2\gamma(t)/r_{max} + C \quad (8)$$

and

$$\Delta P(t)_{min} = 2\Delta\gamma(t)/r_{max} \quad (9)$$

Finally, the drop time $t_{drop}(n)$ can also be plotted as a function of time, $t_{drop}(t)$, using Eq. (4) and Eq. (5). The elimination of C in Eq. (7) and Eq. (9) from Eq. (6) and Eq. (8), respectively, requires minimizing the contribution to pressure change due to analyte viscosity in the capillary tubing between the sensor side-arm and the capillary tip. In the instrument design shown in Fig. 1, the capillary diameter (D_c) has been bored out to 0.020 in. and very short (1.4 cm) to substantially reduce the effect of small changes in the viscosity of the eluate that can change the background pressure signal (1 in. = 2.54 cm). The pressure maximum (Eq. (6)) and pressure minimum (Eq. (8)) both provide a measure of the liquid–air surface tension of each drop of eluate, thus allowing the analysis of materials that lower the surface tension relative to the mobile phase. A decrease in surface tension due to a surfactant eluting will be seen as a decrease in the baseline pressure. Thus, a DSTD chromatogram will contain peaks that decrease from the baseline. To clarify, this is in contrast to our previous report in which a surface tension *lowering* was plotted so the peaks were positive [19]. Since the measured pressure is inversely proportional to drop radius, the sensitivity to surface tension change is significantly higher just when the drop begins to emerge, at $P(t)_{max}$, as compared to prior to drop detachment, or $P(t)_{min}$. It will be shown that $P(t)_{min}$ contains more noise than $P(t)_{max}$ due to small variations in volumetric flowrate and the mechanical stability of the drop. Thus, the overall S/N should considerably favor the $P(t)_{max}$ signal. Note also that $P(t)_{max}$ is independent of eluate density changes, while the drop time-based chromatogram (Eq. (3)) is affected by density, and a mobile phase gradient in HIC will be accompanied by a change in density. This is a significant advantage of pressure-based DSTD [19] over our previous optical designs [15–18].

3. Experimental

3.1. Reagents

A wide variety of surfactants and bulk organic solvents were examined. The solvent 2-propanol (Baker Analyzed, Phillipsburg, NJ, USA), 100% purity by gas chromatography, 1-hexanesulfonic acid (Aldrich, Milwaukee, WI, USA) 98% purity, and *N*-decyl-*N*,*N*-dimethyl-3-ammonio-1-propane-sulfonate (Sigma, St. Louis, MO, USA) >99% purity by thin-layer chromatography, were used as chromatographic standards, injected at 27% (v/v), 980 and 1100 ppm, respectively. Ribonuclease A (EC 3.1.27.5, Sigma) 85% purity, and its impurities were separated by HIC. The injected standard was 2.6 mg/ml, prepared by dissolving 3 mg of ribonuclease A in 1 ml of the initial chromatographic elution buffer. Ribonuclease A at 99% purity (Sigma) was used as a standard in the enzyme assay. Mobile phase buffer solutions were made from ammonium acetate, >99% purity, and ammonium sulfate, 99.3% purity (J.T. Baker, Phillipsburg, NJ, USA) in deionized water.

3.2. Apparatus

Mobile phase was delivered with a dual syringe gradient pump (Microgradient, Brown Lee, Santa Clara, CA, USA) to an injection valve (Model 7125, Rheodyne, Cotati, CA, USA) fitted with an injection loop (5 ml), that introduced samples to the HIC column, 100×2.1 mm I.D. (Synchropak propyl, Micra Scientific, Lafayette, IN, USA). Polyether ether ketone (PEEK) tubing (Upchurch, Oak Harbor, WA, USA), nominally with an I.D. of 0.007 in. (180 μm) by 1/16 in. O.D. was used for making the various connections. The two mobile phase components of the gradient were (A) 0.5 *M* ammonium acetate and 2.0 *M* ammonium sulfate and (B) 0.5 *M* ammonium acetate. HIC gradient separations started at 10% solvent B and 90% solvent A. The mobile phase mixture was ramped to 90% B in 3 min and

was held at 90% B for 4 min to finish each run, and then ramped down to 10% B solvent over 1 min to stabilize for the next run.

The mobile phase then passed through another length of PEEK tubing and was directed through the flow cell (10 μl, 6-mm path) of the UV absorbance detector (250 nm, Model VDM-2, Dionex, Sunnyvale, CA, USA). After absorbance detection the mobile phase then passed through a short length of PEEK tubing (nominally with an I.D. of 0.005 in.) to a zero dead volume PEEK fitting (Upchurch) with a side arm leading to the pressure sensor (Fig. 1) (Validyne Model P305D-20-2369, Northridge, CA, USA) and on through a 1.4-cm stainless steel double bore capillary (machined in-house as in Fig. 1 to reduce the background pressure due to viscosity) where drops form repeatedly at a volumetric flow-rate of 250 μl/min. The pressure sensor converted the differential pressure across a diaphragm into a voltage at 0.02 p.s.i./V, with 10 V full-scale (1 p.s.i. = 6894.75 Pa). The lag volume between the UV absorbance detector and the surface tension detector was 1.3 μl. The stainless steel capillary, initially with a 1/16 in. O.D., was machined and polished with an outside taper ($\alpha = 9°$) to the inside radius of 90 μm, as in Fig. 1, yielding an average baseline drop volume of 8 μl.

3.3. Data collection

Data collection and analysis of the raw $P(T)$ signal (Eq. (1)) was performed at 125 Hz using a Pentium 150 MHz personal computer with a data acquisition board (Model MIO-16B, National Instruments, Austin, TX, USA), using software written in-house. Measurements of the $P(t)_{max}$, $P(t)_{min}$ and $t_{drop}(t)$ as described in the theory were from the raw $P(T)$ signal using software written in-house. For example, after data collection the pressure maximum for each drop (Eq. (6)) was determined by a peak finding algorithm and the data was plotted versus the time of separation (Eq. (4)).

3.4. Enzyme assays

Fractions of the commercially formulated ribonuclease A separated by HIC were collected. The volume of each fraction, dependent on the width of each detected peak, was typically 125 μl. Fractions were concentrated by removing the solvent via lyophilization and reconstituted in 5.2 ml cold water. Separate fractions were assayed for enzyme activity by the spectrophotometric stop rate determination method of Kunitz [24]. Direct fractions were assayed for total protein [25] and triglyceride [26] by automated clinical methods.

4. Results and discussion

Using HIC and pressure-based DSTD, standard chromatographic compounds were used to evaluate instrument performance. Fig. 2 shows the raw pressure signal, $P(T)$, for a standard solution of 1-hexanesulfonic acid eluted in the mobile phase. The first few drops labeled Mobile Phase contain only the elution concentrations of ammonium sulfate and ammonium acetate. Note that each drop produces a maximum and minimum pressure during growth and detachment. The next several drops show lowering of the maximum pressure, and thus the surface tension of the eluate as 1-hexanesulfonic acid is

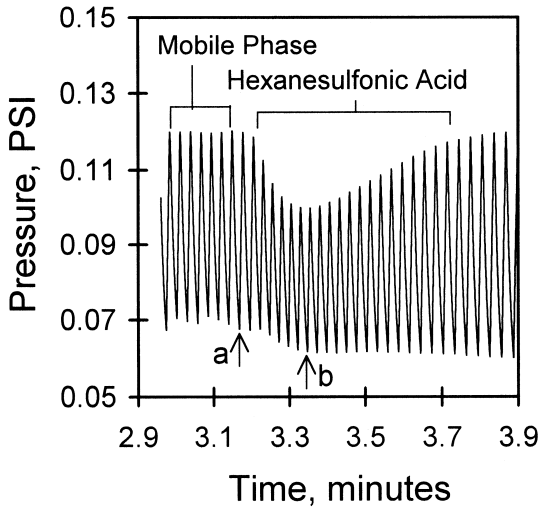

Fig. 2. Raw pressure signal for 1-hexanesulfonic acid in mobile phase, following Eq. (1), that is a portion of the complete separation of the three standards shown in Fig. 5A, with the gradient conditions given in Section 3. Drop profiles for mobile phase and 1-hexansulfonic acid in mobile phase are identified, and a representative drop of each is labeled as 'a' and 'b', respectively, for illustration in Fig. 3A.

eluted from the column. The signal is proportional to concentration to a good approximation over the signal range investigated [15,17,19].

The pressure signal for each drop is referred to as a drop profile as illustrated in Fig. 3A representing an overlay of drop profiles, decomposed from Eq. (1) according to Eq. (2), for mobile phase and 1-hexanesulfonic acid in mobile phase. The actual mobile phase and eluting analyte drop profiles used for Fig. 3A are marked in Fig. 2 as (a) and (b), respectively. The drop time, maximum pressure and minimum pressure are labeled in Fig. 3A for the mobile phase drop profile. Comparing drop profiles (a) and (b), we see a lowering of surface tension as a decrease in P_{max}, P_{min} and t_{drop}. The maximum pressure occurs at the minimum drop radius (Eq. (6)). For a given drop, as the drop grows, the radius increases and the pressure decreases to a minimum that corresponds to drop detachment, i.e., drop time (Eq. (3) and Eq. (8)).

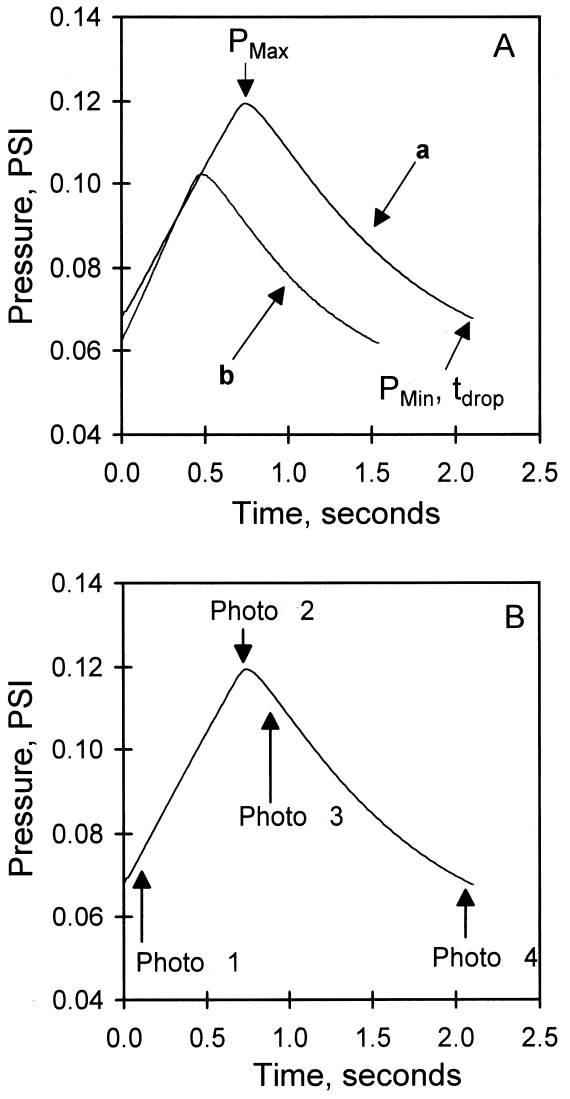

Fig. 3. (A) Overlay of individual drop profiles of mobile phase, a, and 1-hexanesulfonic acid in mobile phase, b, decomposed from the raw signal in Fig. 2 according to Eq. (2). The pressure maximum P_{max}, pressure minimum P_{min}, and drop time t_{drop} for the mobile phase drop profile are labeled. (B) Identification of positions along time axis of mobile phase drop profile a, corresponding to the photographs in Fig. 4.

Special attention was paid toward correlating the physical observations of drop formation and detachment with respect to the observed pressure signal. Photographs in Fig. 4, depict the progress of drop formation and detachment. The water drop and subsequent drop profile used to produce the photographs is detailed in Fig. 3B. Photograph 1 shows the tip just after a drop has fallen. For comparison of dimensions, the capillary at the tip is about 180 μm. Note that there is no residual liquid on the capillary tip, since drop detachment pulls the adhering eluate from the side edges of the tip. This minimizes any band broadening due to hysteresis. Photograph 2 represents the point at which the membrane in the pressure sensor cannot be deformed further without overcoming the surface tension of the eluate at the capillary tip. At this point the maximum pressure of the drop is reached. The surface tension of the relatively small hemisphere is broken and the flow rapidly forces the liquid into a full sphere (photograph 3). During drop growth the wetting of the outside edge of the tip to a distance of approximately 40 μm was observed. The drop now increases in size and begins to elongate. Photograph 4 shows the drop just before detachment (maximum drop radius and minimum pressure). Note that most of the drop in photograph 4 is out of the field of view. Drop detachment completes the cycle for one drop, pulling the wetting liquid from the capillary side and returning to the condition in photograph 1.

Observation of the drop time and pressure data generated from the separation of known surface active materials will allow us to understand how to optimize the S/N of the data obtained from gradient

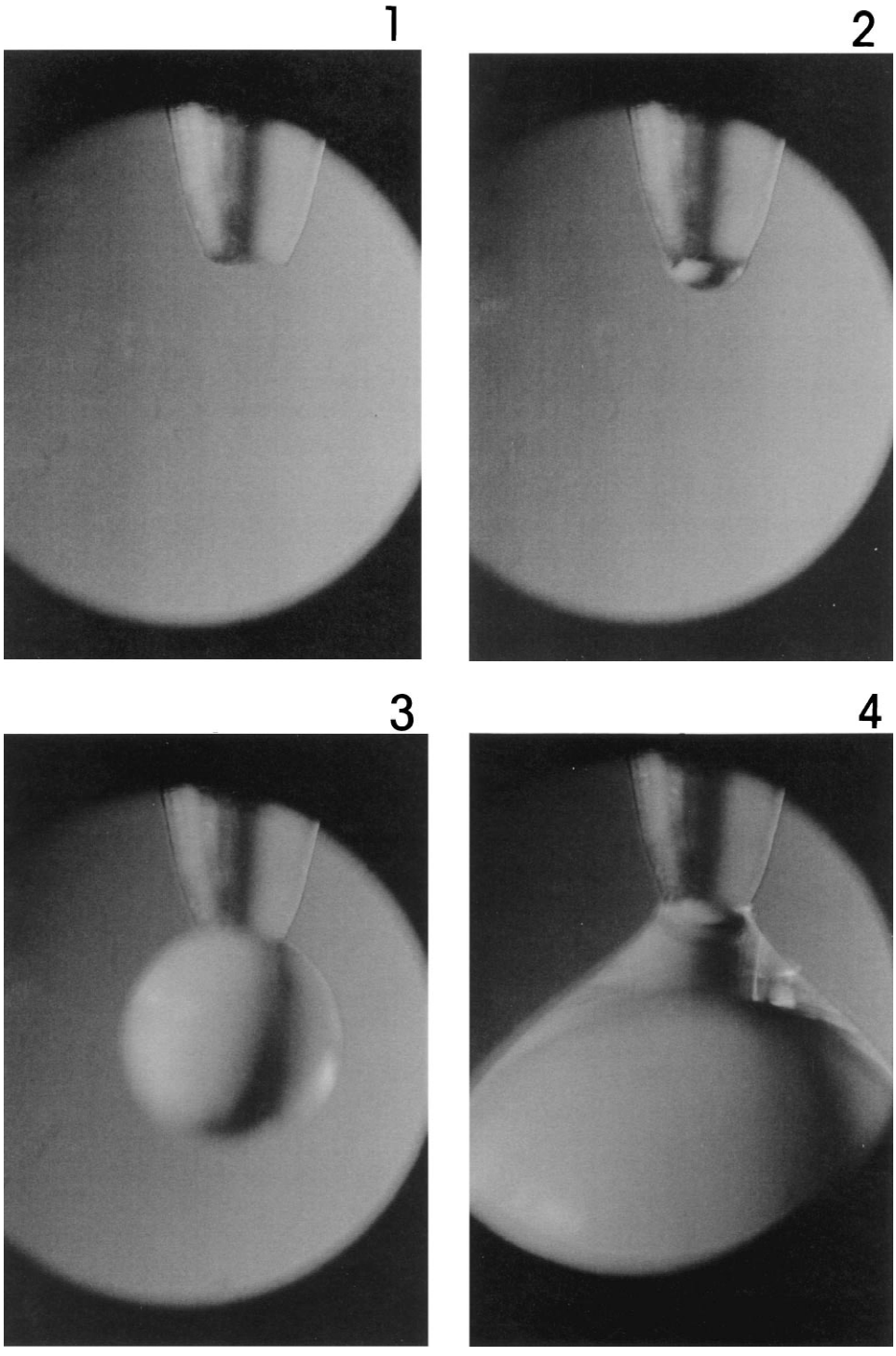

Fig. 4. Photographs of the capillary tip and eluate drop at the four stages of development as identified with the drop profile signal in Fig. 3B.

HIC separations. First we will examine the $P(t)_{max}$ signal (Eq. (6)). In Fig. 5A we see the HIC separation of three test analytes that all lower the surface tension of the mobile phase as detected with the DSTD: isopropyl alcohol, 1-hexanesulfonic acid and *N*-decyl-*N*,*N*-dimethyl-3-ammonio-1-propane sulfonate (DDAPS). A portion of the raw pressure signal used to prepare Fig. 5A was shown in Fig. 2. The chromatogram shown in Fig. 5B has $t_{drop}(t)$, (Eq. (3) and Eq. (4)), plotted as a function of the time of

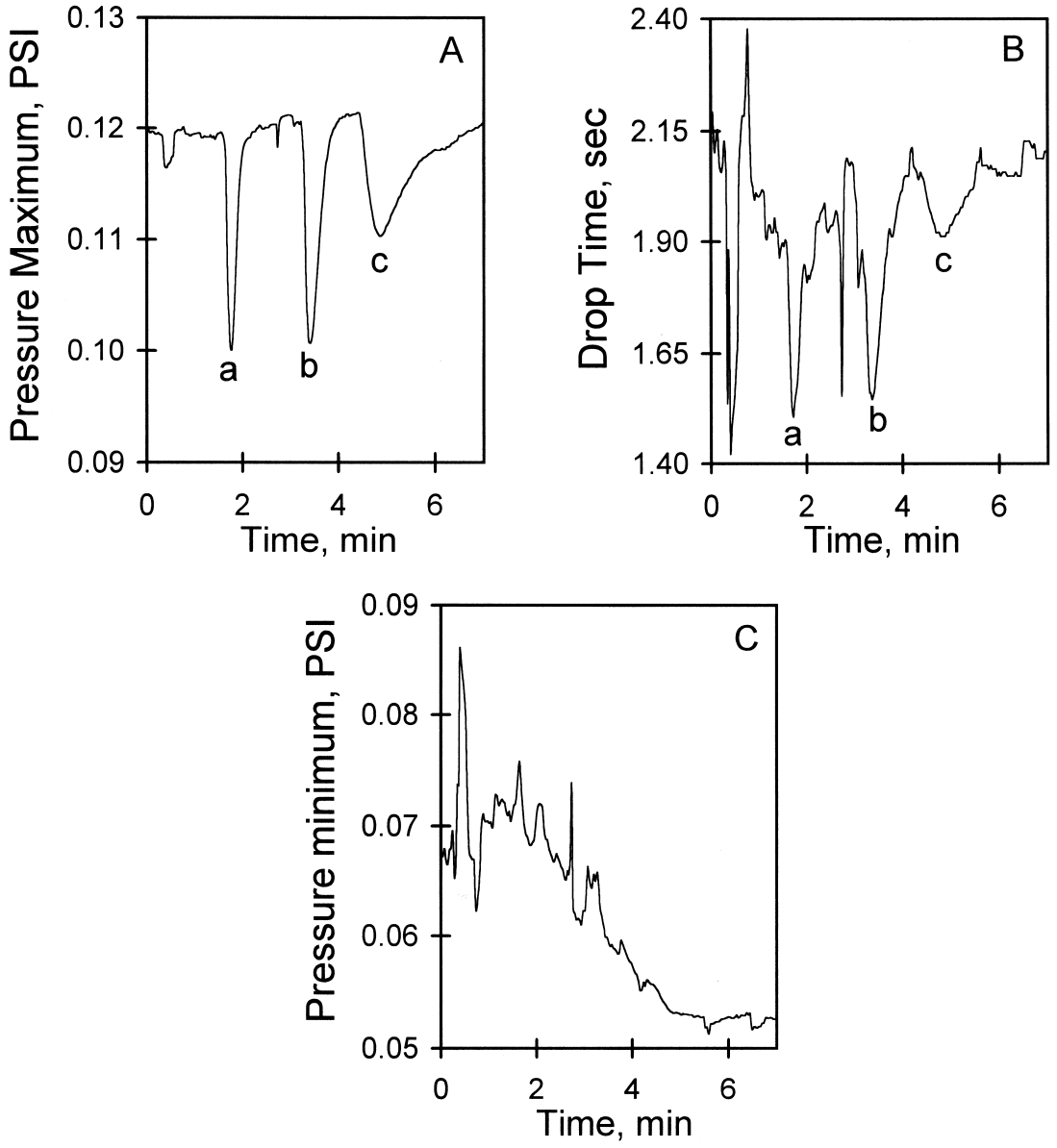

Fig. 5. HIC separation and dynamic surface tension detection (DSTD) using three data analysis methods and the mobile phase gradient given in Section 3 of (a) isopropyl alcohol, (b) 1-hexanesulfonic acid and (c) *N*-decyl-*N*,*N*-dimethyl-3-ammonio-1-propane sulfonate (DDAPS): (A) signal plotted is maximum pressure $= P(t)_{max}$, Eq. (6); (B) signal plotted is drop time $= t_{drop}(t)$, Eq. (3); (C) signal plotted is pressure minimum $= P(t)_{min}$, Eq. (8). Note the the S/N in (C) is so poor that the analyte peaks cannot be identified.

separation. Note that the drop time-based signal has a much lower signal-to-noise ratio than the pressure maximum plot. Likewise, in Fig. 5C the $P(t)_{min}$ chromatogram (Eq. (8)) is at such poor S/N, for reasons outlined in the theory section, that analyte peaks are not observed. In experiments presented here and in those from earlier studies [19] the pressure minimum for each drop was found to have a sensitivity of approximately 15 times less than the pressure maximum for changes in the liquid–air surface tension (data not shown for brevity). This difference in sensitivity, in close agreement with the theoretical sensitivity, is simply the inverse ratio of the radii, r_{max}~1000 μm versus r_{min}~90 μm (capillary tip inside radius). Fig. 5A–C also provides insight into the origin of the noise levels seen in each chromatogram. The baseline noise was three times worse for $P(t)_{min}$ compared to $P(t)_{max}$ based upon measurements of background gradient runs without sample injection. Many of the features in the $P(t)_{min}$ chromatogram correspond to the inverse of noise in the drop time-based chromatogram. As the flow-rate fluctuates due to gradient pumping 'noise', $t_{drop}(t)$ was inversely affected as compared to $P(t)_{min}$. Meanwhile, the pressure noise observed for $P(t)_{max}$ was at a minimum because at the moment in time of the $P(t)_{max}$ measurement within each drop, the flow-rate is actually changing direction with respect to the sensor membrane, and is essentially zero. Whereas, at $P(t)_{min}$ the flow direction is moving away from the sensor membrane. Another contributing factor may be the drop stability as a function of its size and shape. At the point of maximum pressure the drop is at a minimum radius (photograph 2). The conformation of the drop when it is at the minimum radius is more mechanically stable than the drop at the maximum radius (photograph 4). Mechanical stability may also be coupled to the flow-rate variation in determining the noise levels. The combination of lower noise and higher sensitivity results in $P(t)_{max}$ having a S/N about 45 times larger than for $P(t)_{min}$.

The gradient HIC–DSTD methodology, coupled with UV absorbance detection, was applied to the analysis of a commercial ribonuclease A formulation. Ribonuclease A (85% purity) was separated from its contaminants by HIC with UV absorbance detection and DSTD in series to monitor the separation. The UV absorbance trace is shown in Fig. 6A.

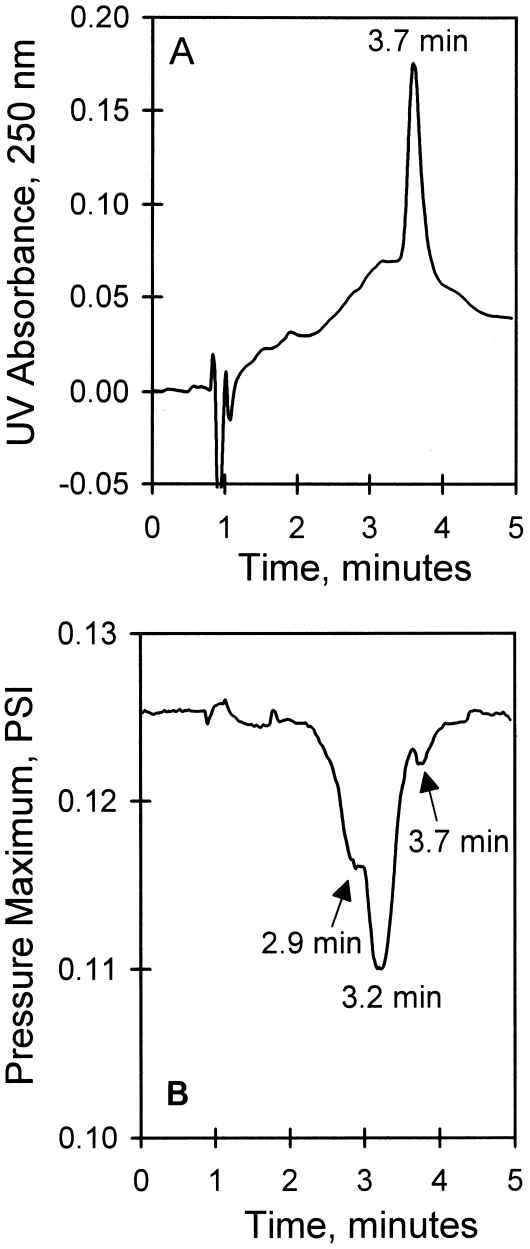

Fig. 6. Separation of ribonuclease A (85% purity) from its contaminants by HIC with UV absorbance detection and DSTD, with the gradient the same as in Fig. 5: (A) UV absorbance signal for the separation that has been corrected by subtracting the background due to the gradient program without sample injection. The peak at 3.7 min was identified as ribonuclease A. (B) DSTD signal ($P(t)_{max}$) from the same separation, showing three surface tension lowering peaks with retention times of 2.9, 3.2 and 3.7 min.

Note the single strongly absorbing peak at 3.7 min. Fig. 6B shows the DSTD signal ($P(t)_{max}$) from the same separation, showing three peaks with retention times of 2.9, 3.2 and 3.7 min. Peak fractions from each chromatographic peak were collected and tested for enzyme activity. The surface active peaks at 2.9 and 3.2 min showed no enzyme activity, while the peak at 3.7 min showed activity of approximately 9 units/mg lyophilized material. The expected activity of ribonuclease A was 51 units/mg protein, as provided by Sigma. The absorbance peak height observed for ribonuclease A (3.7 min in Fig. 6B) indicated a 100% (±10%) recovery based upon UV absorbance calibration of a standard. Thus, the reduction in activity was attributed to the lyophilization process. The surface tension peak at 3.7 min, identified by enzyme assay as ribonuclease A, is smaller than the contaminants. Ribonuclease A has been shown to have modest surface activity when compared to other members of the globular protein class, especially in this time domain [27]. The relative surface tension lowering of the 3 mg/ml ribonuclease A was estimated to be 0.02 $\Delta\gamma/\gamma$ per μg of protein injected. This is approximately equivalent to the surface tension lowering that would occur with a 0.75% aqueous solution of 2-propanol. Reinjection of the lyophilized fraction from the peak at 3.7 min, reconstituted in 100 μl did not show peaks at 2.9 and 3.2 min, indicating that the contaminating surface active species had been removed by the chromatographic process. The polarity range corresponding to the peaks at 2.9 and 3.2 min is similar to that of 1-hexanesulfonic acid. The signal of the largest peak at 3.2 min is comparable to 80 ppm 1-hexanesulfonic acid at the detector, although surface activity, and hence detectability, varies widely amongst compounds within this polarity class. Analysis of the fractions encompassing the 2.9- and 3.2-min peaks for total protein and triglyceride content excluded these classes of compounds below the 2-μg/ml (total protein) and 1-μg/ml (triglyceride) concentrations.

Many enzyme recovery and purification methods use surface active materials for the purpose of solubilization. Methods for purifying proteins and other biological materials from recombinant bacterial hosts invariably start with breaking the bacterial cells open. A typical crude broken cell preparation contains membranes, cellular organelles, and a large number of soluble molecular species, all dispersed in an aqueous buffered solution [28]. Surfactants are routinely used in the processing of large quantities of protein as flow improvers and solubilizing agents. Other synthetic additives that may affect surface tension are anti-foaming materials and ion pairing agents [28]. These, and many other compounds, make up the various classes of surfactants that, even at low concentrations, affect surface active properties. Recombinant protein products purified by preparative chromatography are accompanied by closely eluting and chemically related compounds. Therefore, surface active species in the ribonuclease formulation may also be endogenous to the cells from which the protein was purified. All of these are potential sources of the surface active species found in the ribonuclease sample analyzed.

Thus, the information generated by HIC coupled to DSTD, which is highly selective for materials that lower the liquid–air surface tension of aqueous systems, is quite useful in the analysis of materials derived from biological sources. For the purposes of studies involving large molecule dynamics, the presence of surfactants can cause the hydrophobic regions of the molecule being studied to be more soluble in the surrounding water or buffer. Thus, the detection of even a small concentration of surfactants in biological polymer research would be of great use. Our technique shows much promise in this area with low detection limits [19] and high selectivity for materials that lower the surface tension of aqueous systems. Future work will focus on obtaining kinetic information for each drop profile. A pressure sensor with a significantly faster time response will be required [13,14]. A pumping system that exhibits less noise will also be required. A broader range of proteins can then be examined to determine their kinetic surface tension properties during chromatographic elution.

Acknowledgements

This work was supported in part through a grant from the American Association of Clinical Chemistry Van Slyke Society Research Award (K.J.S.). We thank Max J. Kopp of Validyne for technical support

through use of the pressure sensor and Carsten A. Bruckner for software assistance.

References

[1] A.W. Adamson, Physical Chemistry of Surfaces, 5th ed., Wiley-Interscience, New York, 1990.
[2] D. Myers, Surfaces, Interfaces, and Colloids: Principles and Applications, VCH, New York, 1991.
[3] D. Zhou, D. Pietrzyk, Anal. Chem. 64 (1992) 1003.
[4] S.A. Maki, J. Wanges, N.D. Danielson, Anal. Chem. 64 (1992) 583.
[5] R. Nagarajan, D.T. Wasan, J. Colloid Interface Sci. 159 (1993) 164.
[6] G. Serrien, G. Geeraerts, L. Ghosh, P. Joos, Colloids Surf. 68 (1992) 219.
[7] G. Enhorning, J. Appl. Physiol.: Respirat. Environ. Exercise Physiol. 43(2) (1977) 198.
[8] D.R. Ward, P.R. Garrett, J. Colloid Interface Sci. 132 (1989) 475.
[9] K. Lunkenheimer, G. Serrien, P. Joos, J. Colloid Interface Sci. 134 (1990) 407.
[10] D.R. Otis Jr., E.P. Ingenito, R.D. Kamm, M. Johnson, J. Appl. Physiol. 77 (1994) 2681.
[11] N.D. McMillan, E. O'Mongain, J. Walsh, L. Breen, D.G.E. McMillan, M.J. Power, J.P. O'Dea, S.M. Kinsella, M.P. Kelly, C. Hammil, D. Orr, Opt. Eng. 33 (1994) 3871.
[12] K. Hool, B. Schuchardt, Meas. Sci. Technol. 3 (1992) 451.
[13] C.A. MacLeod, C.J. Radke, J. Colloid Interface Sci. 160 (1993) 435.
[14] C.A. MacLeod, C.J. Radke, J. Colloid Interface Sci. 166 (1994) 73.
[15] L.R. Lima, D.R. Dunphy III, R.E. Synovec, Anal. Chem. 66 (1994) 1209.
[16] L.R. Lima III, R.E. Synovec, J. Chromatogr. A 691 (1995) 195.
[17] T.E. Young, R.E. Synovec, Talanta 43 (1996) 889.
[18] M.L. Shulman, M.C. Jacobson, R.J. Charlson, R.E. Synovec, T.E. Young, Geophys. Res. Lett. 23(3) (1996) 277.
[19] N.A. Olson, R.E. Synovec, W.B. Bond, D.M. Alloway, K.J. Skogerboe, Anal. Chem. 69 (1997) 3496.
[20] B. Miller, I. Tyomkin, J. Adhes. Sci. Technol. 6 (1992) 1371.
[21] M.T.S.D. Vasconcelos, M.A.G.O. Azenha, O.M. Lage, Anal. Biochem. 241 (1996) 248.
[22] Y. Gao, Y.X. Zheng, Acta Chim. Sinica 54 (1996) 504.
[23] B. Konig, U. Dietrich, G. Klose, Langmuir 13 (1997) 525.
[24] M.J. Kunitz, Biol. Chem. 164 (1946) 563.
[25] C.A. Pennock, L.P. Passant, F.G. Bolton, J. Clin. Pathol. 21 (1968) 518.
[26] J.D. Batjer, G. Kroon, R.J. Liedtke, A.M. Zebelman, Clin. Chem. 30 (1984) 989.
[27] B.C. Tripp, J.J. Magda, J.D. Andrade, J. Colloid Interface Sci. 173 (1995) 16.
[28] G. Zubay, Biochemistry, 2nd ed., Macmillan, New York, 1988.